

1 Fabrication of Biomimetically Patterned Surfaces and Their 2 Application to Probing Plant–Bacteria Interactions

3 Boce Zhang,^{†,‡} Yaguang Luo,^{*,‡,§} Arne J. Pearlstein,^{||} Jesse Aplin,^{†,‡} Yi Liu,[⊥] Gary R. Bauchan,[#]
4 Gregory F. Payne,^{⊥,Δ} Qin Wang,[†] Xiangwu Nou,[‡] and Patricia D. Millner[‡]

5 [†]Department of Nutrition and Food Science, [⊥]Institute for Bioscience and Biotechnology Research, ^ΔFischell Department of
6 Bioengineering, University of Maryland, College Park, Maryland 20742, United States

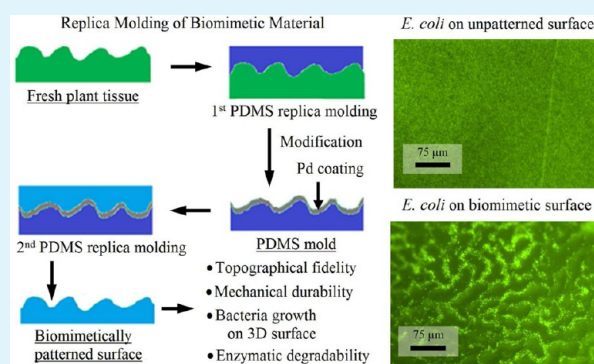
7 [‡]Environmental Microbial and Food Safety Lab, Agricultural Research Service, [§]Food Quality Lab, Agricultural Research Service, and

8 [#]Electron and Confocal Microscopy Unit, Agricultural Research Service, United States Department of Agriculture, Beltsville,
9 Maryland 20705, United States

10 ^{||}Department of Mechanical Science and Engineering, University of Illinois at Urbana–Champaign, Urbana, Illinois 61801, United
11 States

12 **ABSTRACT:** We have developed a two-step replica molding
13 method for rapid fabrication of biomimetically patterned plant
14 surfaces (BPS) using polydimethylsiloxane (PDMS-BPS) and
15 agarose (AGAR-BPS). Beyond providing multiple identical speci-
16 mens that faithfully reproduce leaf surface microstructure, this
17 approach also offers unique chemical, physical, and biological
18 features. PDMS-BPS provide good structural durability for SEM
19 examination, have surface wettability comparable to plant surfaces
20 for coating development, and allow for real-time monitoring of
21 biosynthesis through incorporation into microfluidic devices.
22 AGAR-BPS are compatible with bacterial growth, recovery, and
23 quantification, and enable investigation of the effects of surface
24 topography on spatially varying survival and inactivation of
25 *Escherichia coli* cells during biocide treatment. Further development and application of these biomimetically patterned surfaces
26 to study (and possibly modify) other aspects of plant–bacteria interactions can provide insight into controlling pathogen
27 contamination in a wide range of applications.

28 **KEYWORDS:** plant–bacteria interaction, biomimetically-patterned surfaces, replica molding, PDMS, agarose, surface topography



29 ■ INTRODUCTION

30 Consumption of pathogen-contaminated food is a major cause
31 of human illness and mortality. The Centers for Disease
32 Control and Prevention (CDC) reports that nearly 48 million
33 illnesses, more than 128 000 hospitalizations, and more than
34 3000 deaths are attributable to foodborne disease each year in
35 the U.S. alone.¹ Fresh leafy green vegetables (e.g., lettuce,
36 spinach, cabbage) have emerged as a substantial vehicle of
37 foodborne bacterial pathogens, despite use of bactericidal
38 sanitizers (chiefly chlorine) in processing wash water.² Evidence
39 strongly indicates that bacterial cells persist to varying degrees
40 on and in tissues of leafy greens. Although internalized
41 contamination originating from seeds and roots is reportedly
42 rare,^{3–6} leaves, with their rough and hydrophobic surface
43 microstructures, including stomata, hydathodes, and trichomes,
44 provide protected harborage for bacterial cells in disinfecting/
45 sanitizing washing processes.^{3–10}

46 The importance of surface attachment, and the extent to
47 which local topography and hydrophobicity affect attachment,
48 is evident in the kinetics of bacterial disinfection by chemical
49 sanitizers, where unattached and loosely attached bacteria are

50 easily inactivated, and bacteria strongly attached to a surface are
51 far less vulnerable.^{7–9} Unfortunately, the specific mechanisms
52 of attachment/detachment involved in these microscale plant–
53 bacteria surface interactions, and the surface attributes and
54 interfacial forces that affect attachment/detachment, are not
55 understood.^{3,7–9} As a result, development of improved
56 mitigation approaches (e.g., involving nonchlorinated sanitizers,
57 surfactants, and ultrasound) is highly empirical.

58 A significant impediment to understanding plant–bacteria
59 surface interactions is that the surface microstructure of leaves
60 varies with species, cultivar, plant, and location on the plant,
61 and is also influenced by growing conditions and maturity stage.
62 These factors make it difficult to replicate experiments, and to
63 interpret variation as a function of experimental parameters.
64 Development of biomimetically patterned surfaces (BPS) that
65 faithfully and reproducibly capture the microstructural top-
66 ography of plant leaves provides a means to precisely replicate

Received: April 19, 2014

Accepted: July 9, 2014

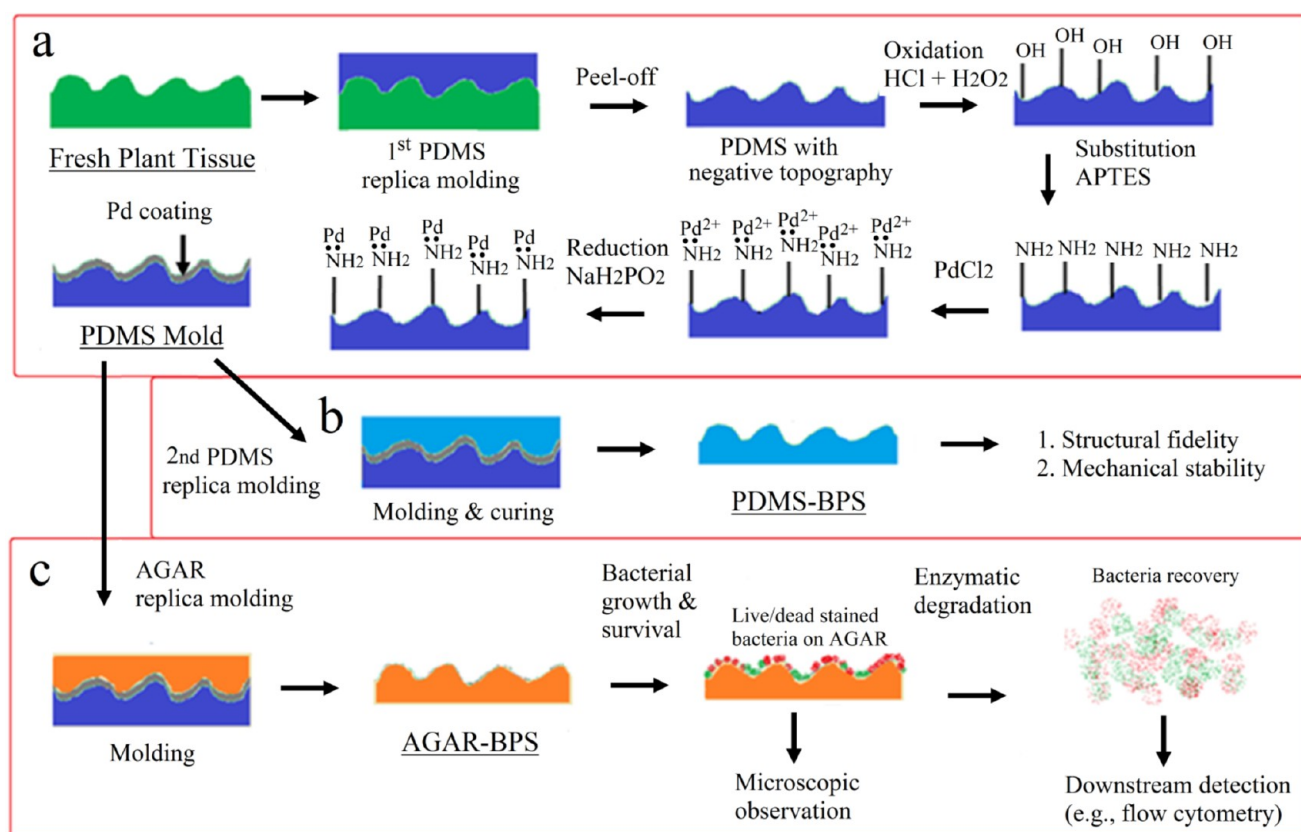


Figure 1. Schematic presentation of BPS fabrication via replica molding: (a) replica molding and chemical modification of Pd-coated PDMS stamp to produce final PDMS mold; (b) thermal molding of PDMS-BPS; (c) thermal molding of AGAR-BPS.

67 experiments, allowing interpretation of the results when
68 parameters are systematically varied, without confounding
69 influences of natural variation. Moreover, the capability to
70 tailor and characterize surface microstructures (and other
71 surface properties, such as hydrophobicity) will enable
72 experiments that enhance understanding of the interactions
73 between plant surfaces and human pathogens (including those
74 interactions relevant to mitigation strategies), as well as with
75 phytopathogens.

76 Although artificial surfaces with deliberately patterned micro-
77 or nanoscale texture are frequently used to study attachment,
78 growth, and migration of mammalian cells, a recent review¹¹
79 mentions very few previous reports on the use of reproducible
80 surfaces in studies of microbial attachment. Apoga et al.¹²
81 studied appressorial attachment of fungal germlings to regular
82 arrays of pillars on a silicon substrate, as a function of pillar
83 area, and found that essentially no appressoria were induced
84 below a minimum area of the flat pillar end. Held et al.¹³
85 studied attachment of wild-type and mutant *Neurospora crassa*
86 to unpatterned surfaces in microfluidic channels. De la Fuente
87 et al.¹⁴ used an unpatterned polydimethylsiloxane (PDMS)
88 surface in a microfluidic channel to study attachment of a
89 pathogenic grapevine bacterium, and measured very different
90 detachment forces for wild-type and mutant organisms. Finally,
91 Sirinutombon et al.¹⁵ used microfabricated silicon surfaces to
92 study attachment of *Escherichia coli* to trichome and stomatal-
93 like structures, and grooves between epidermal cells. Each 2 cm
94 square Si specimen had a spatially periodic array of only one of
95 these features, and each feature type had a geometrically simple
96 topography. These authors found strong localization of
97 attached bacteria at the bases of the trichome-like structures.

For the stomatal-like structures, bacteria localized much more
98 strongly at a certain “stand-off” distance (i.e., neither close to
99 nor far from the “stomata”), whereas for grooves no localization
100 was observed.
101

In none of this work was the surface hydrophobicity, the
102 nanoscale texture, or any other surface property (other than the
103 microscale topography) varied. The capability to simulta-
104 neously control microscale topography and surface properties
105 like hydrophobicity, on a reproducible surface, provides the
106 opportunity to examine plant–bacteria surface interactions
107 relevant to food sanitization, including how attachment and
108 detachment are impacted by environmental matrices.
109

In the present work, we move beyond the previous use of
110 surfaces having simple, highly ordered microstructures with a
111 high degree of symmetry.¹⁶ We first demonstrate that replica-
112 molding using rapid fabrication techniques (Figure 1) produces
113 PDMS- and agarose-based (AGAR) biomimetically patterned
114 surfaces (BPS) having the microstructural topography of a
115 spinach leaf. In addition to microstructural fidelity, we show
116 that these PDMS-BPS have sufficient mechanical integrity
117 under vacuum conditions to allow for electron microscopy. We
118 also demonstrate that PDMS-BPS have surface wettability
119 characteristics comparable to those of a natural plant tissue,
120 which will aid in the conduct of replicable studies involving the
121 interaction of surface properties and microstructure. Finally, we
122 show that AGAR-BPS with added nutrients provide the
123 capability to study growth and survival of bacteria on a
124 topographically structured surface, and explore the possibility of
125 recovering live and dead bacterial cells via enzymatic
126 degradation and flow cytometry.
127

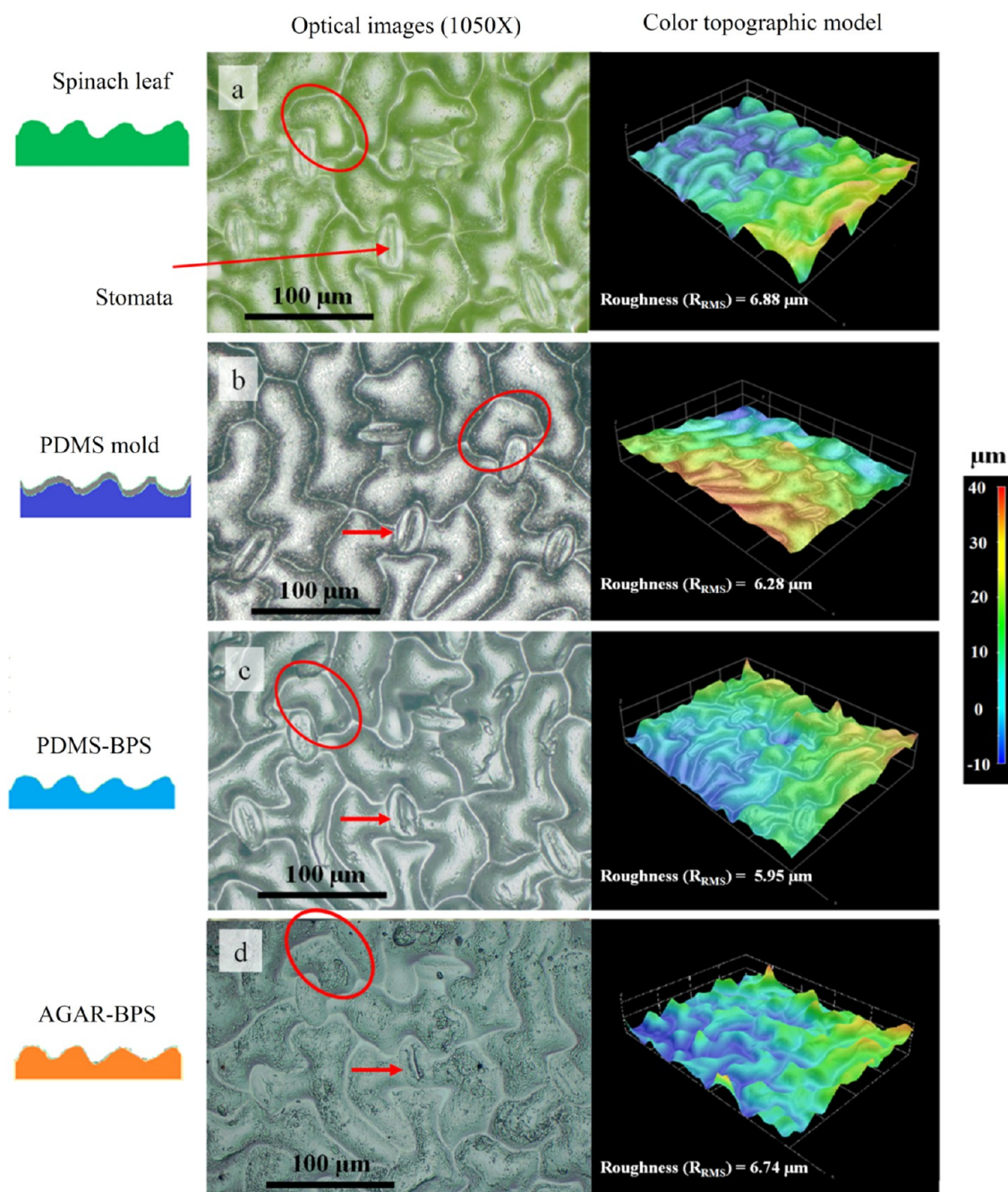


Figure 2. Hirox 3D microscopy images and 3D topographical models show faithful replication of surface topography. (a) Spinach leaf; (b) Pd-coated PDMS stamp; (c) PDMS-BPS; (d) AGAR-BPS. Red circles and arrow highlight the near-identical plant cell morphology, and stomatal structure, respectively, on the surfaces.

128 ■ RESULTS AND DISCUSSION

129 Microstructural Characterization of PDMS Stamps 130 and Biomimetically Patterned Surfaces.

131 After preparation
132 of these artificial surfaces, as described in Materials and
133 Methods, it was important to establish that they faithfully
134 reproduced the surface topography of spinach leaves. A Hirox
135 3D microscope was used to perform 3D imaging of these
136 surfaces. Figure 2 shows optical images and color topographic
137 renderings of (a) the original spinach leaf, and the
138 corresponding areas of (b) the final Pd-coated PDMS stamp
139 (hereinafter referred to as the PDMS mold), (c) the PDMS-
140 BPS, and (d) the AGAR-BPS. The PDMS mold in Figure 2b
141 showed structure and topography mirroring (i.e., opposite to

141 that of) the spinach leaf (Figure 2a). Panels c and d in Figure 2
142 show the PDMS-BPS and AGAR-BPS replicas of the leaf, 142
143 respectively, made using the PDMS mold. They are mirror 143
144 images of the PDMS mold, and clearly provide true replicas of 144
145 the surface topographical features (e.g., valleys between built-up 145
146 cellular structures, etc.) of the original spinach leaf (Figure 2a). 146
147 These images suggest that surface microstructures of epithelial 147
148 cells were faithfully reproduced via replica molding. The root- 148
149 mean-square roughness (R_{RMS}) of the surfaces (examples of 149
150 which are shown in Figure 2) was measured using the standard 150
151 deviation of the z-values of all pixels (1.92 million pixels over an 151
152 area of $300 \mu\text{m}$ by $200 \mu\text{m}$). The results are quite similar for all 152
153 four surface types, consistent with the hypothesis that, at this

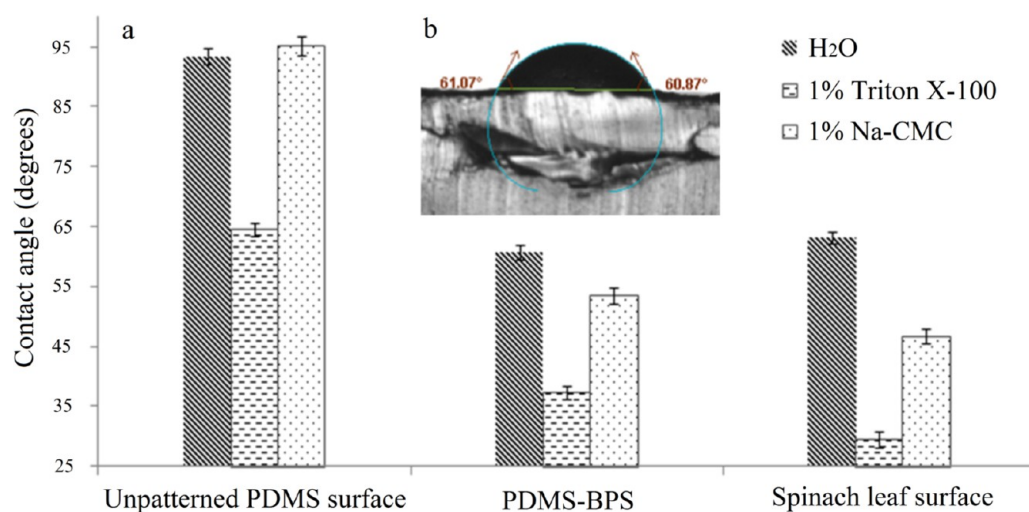


Figure 3. Surface wettability of unpatterned PDMS, PDMS-BPS, and spinach leaf surface for surfactant and coating development. (a) Contact angle measurement (mean \pm standard deviation) of water, 1% aqueous solution of Triton X-100, and 1% aqueous solution of Na-CMC. (b) Snapshot of contact angle measurement using sessile drop method (e.g., water on PDMS-BPS).

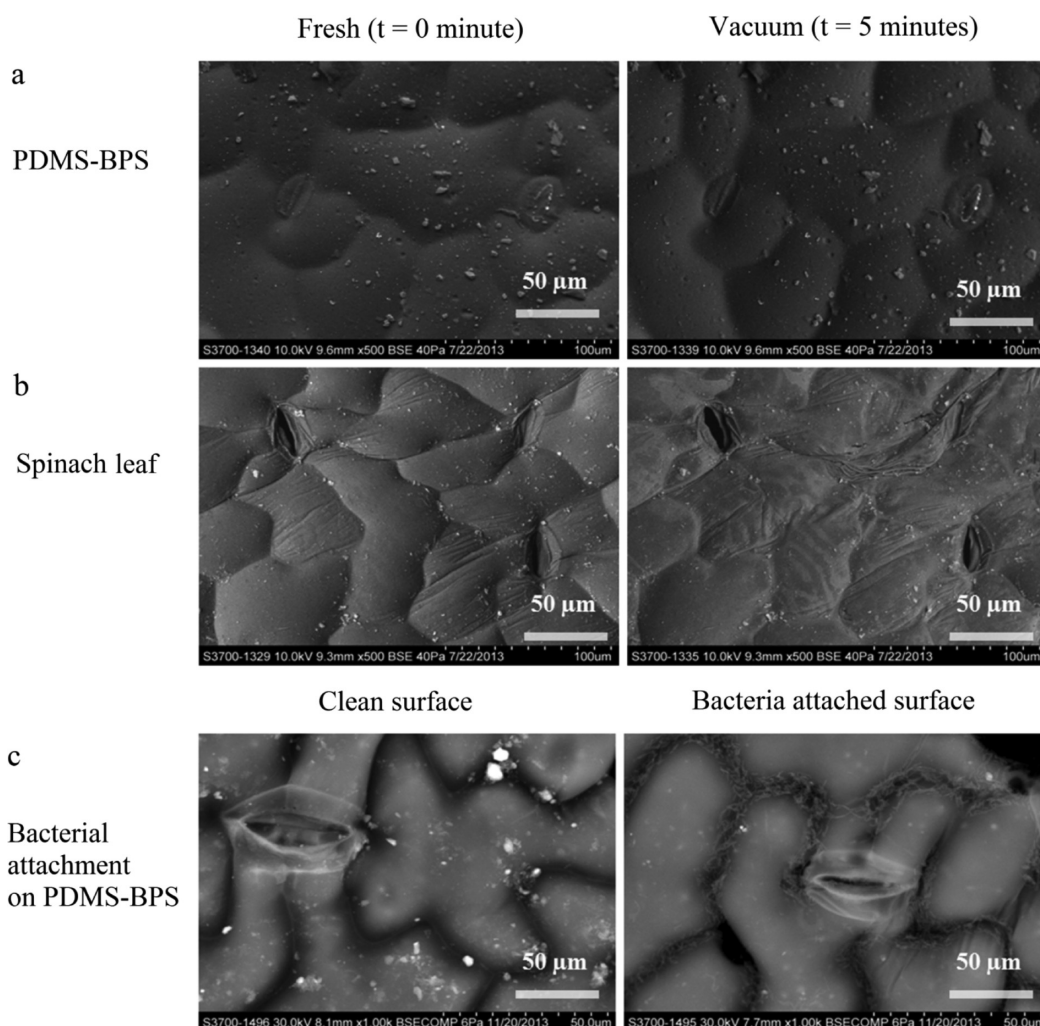


Figure 4. VP-SEM images (500 \times , -25.0 $^{\circ}$ C, and 10.0 kV): (a) PDMS-BPS; (b) spinach leaf. Results show that at 40 Pa vacuum, PDMS-BPS is structurally more stable than spinach leaf. (c) Effect of natural topography on bacterial attachment for PDMS-BPS.

154 resolution, the topographies of the real leaf and of the PDMS
 155 and AGAR biomimetically patterned surfaces, are very similar.
 156 Much of the variation of R_{RMS} among the different surfaces can

be attributed to glare on a glossy surface (e.g., through large
 157 apparent peaks or depressions at the edges of the images); and
 158 environmental humidity, which can also affect leaf plumpness
 159

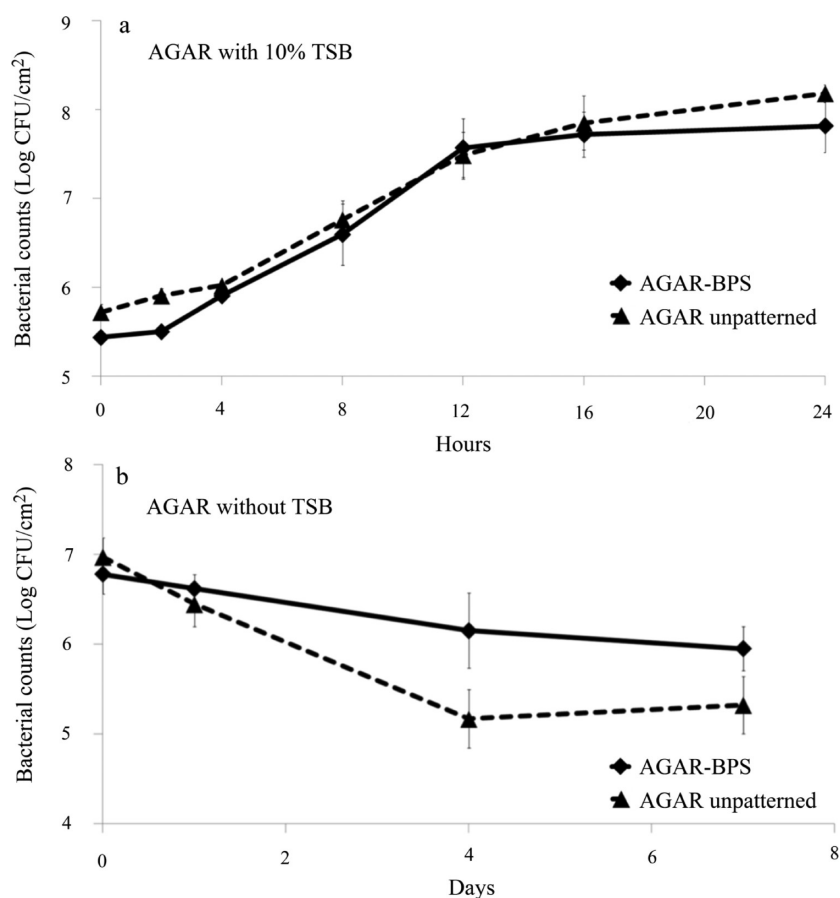


Figure 5. Effect of topography on bacterial growth and survival: (a) bacterial growth on unpatterned and AGAR-BPS with 10% TSB supplement; (b) bacterial survival on AGAR surface without TSB supplement.

160 and the AGAR-BPS surfaces because of either saturation or
161 dehydration.

162 **Wettability of PDMS Biomimetically Patterned Surfa-**
163 **ces.** PDMS offers the possibility of altering surface physical
164 characteristics while maintaining durable mechanical and
165 transparent optical properties, thus providing insight into
166 plant–bacteria interaction. We first evaluated the potential of
167 PDMS-BPS for in vitro study of plant–bacteria interaction in
168 terms of the potential to provide surface wettability comparable
169 to the natural plant tissue surface, and structural stability in
170 vacuum (VP-SEM).

171 The surface wettability of spinach leaf, unpatterned PDMS,
172 and PDMS-BPS was evaluated by contact angle measurement
173 on static sessile drops using an optical tensiometer. The inset
174 image in Figure 3 shows contact angles of water, aqueous
175 solutions of Triton X-100 (a nonionic surfactant), and Na-
176 CMC (sodium carboxymethylcellulose, a cellulosic gum used as
177 an edible coating material, thickener, and emulsion stabilizer)
178 on these solid surfaces. We can identify three possible
179 contributors to variance in the contact angle measurements:
180 (a) contact angle hysteresis, in which the measured contact
181 angle of a static drop might differ according to whether the
182 interface has most recently advanced or receded; (b) random or
183 systematic experimental error, including error associated with
184 measurement precision, electronics, vibration, temperature
185 variation, etc.; and (c) for the patterned surfaces, precise
186 location of the drop on the surface. The fact that the variance is
187 small for each combination of surface and liquid suggests that
188 contact angle hysteresis is not very important for any of these

189 combinations, and that small variations in drop position on the
190 patterned surface and leaf are not important for those cases.

191 The unpatterned PDMS surface was hydrophobic to water
192 and to the Na-CMC solution, with contact angles near 90°. Triton X-100 improves the surface wettability of hydrophobic
193 surfaces by reducing the contact angle to 65°, consistent with
194 previous work.¹⁷ Compared to unpatterned PDMS, biomimeti-
195 cally patterned PDMS surfaces showed much better wettability
196 (corresponding to reductions of 32, 42, and 43% for water,
197 Triton X-100, and Na-CMC, respectively) for drops of all three
198 liquids, probably due to the Cassie impregnating wetting state
199 (the “petal” effect, in which liquid wets large but not small
200 grooves, where adhesive forces between the liquid and solid are
201 very high),^{18–20} and the formation of air pockets in the valleys
202 between asperities. For these three liquids, the considerably
203 smaller differences between the wettability of PDMS-BPS and
204 that of spinach leaf (about 5, 12, and 22% for water, Triton X-
205 100, and NaCMC, respectively) show the importance of
206 topography, and suggest significant potential for use of
207 biomimetically patterned surfaces of PDMS in rapid screening
208 of surfactants and coating materials of interest in applications.
209 The ability to replicate different leaf microstructures provides
210 the capability to better understand how topographical features
211 of real biological materials affect wettability. Since both surface
212 biochemistry and topography are critical to bacterial attach-
213 ment, growth, and inactivation, the present approach allows for
214 a relatively “clean” separation of the effects of surface
215 microstructure from those of surface chemistry and nanoscale
216 texturing. Independent control of the chemical composition 217

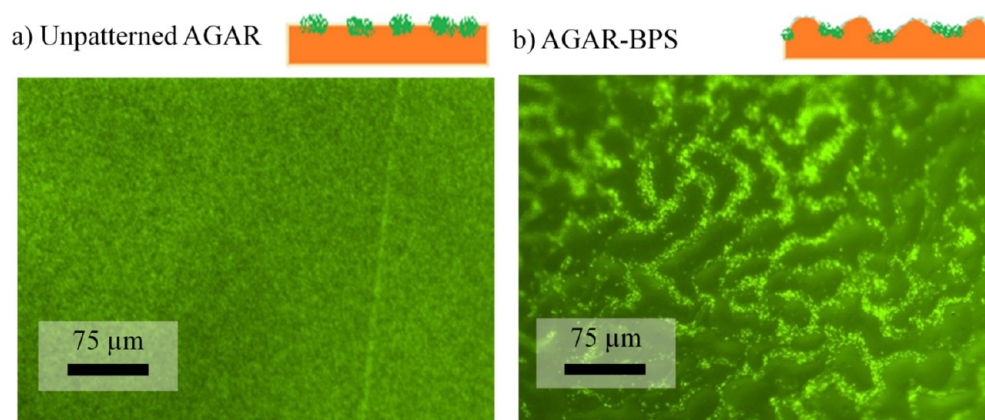


Figure 6. Fluorescence images (100 \times) of live (green) stained *E. coli* growth on AGAR surface showing effects of topography on bacterial growth: (a) unpatterned AGAR surface after 6 h incubation; (b) AGAR-BPS after 6 h incubation.

and properties of the polymeric surface, while maintaining identical microstructures in the replica-molding process, will be the next step.

SEM Compatibility of PDMS Biomimetically Patterned Surfaces. Because studies of surface topography and structure using SEM and other imaging technologies typically require a high-vacuum environment, we evaluated the structural stability of PDMS-BPS under vacuum conditions in a variable-pressure SEM (VP-SEM). The SEM images indicate that PDMS-BPS (Figure 4a) were robust and very durable in the VP-SEM, and that all topographic features were preserved during vacuum exposure, while the epithelial cells of actual spinach leaf (Figure 4b) collapsed after 5 min at low (40 Pa) vacuum.

The SEM compatibility of PDMS-BPS was used to investigate bacterial attachment, and to provide insight into how natural topography affects bacterial distribution on plant surfaces. Figure 4c shows that bacterial cells tend to concentrate in valleys. This result suggests that the solution in which bacteria are suspended can provide sufficient wetting, despite the hydrophobic nature of both the PDMS surface and the natural spinach tissues. Therefore, transition to the Cassie impregnating wetting state could explain how an aqueous bacterial suspension interacts with natural topography on plant surfaces.²¹ The in vacuo stability of the PDMS-BPS strongly suggests that such surfaces can be a valuable tool for detailed SEM examination of plant surface topography, by significantly shortening and simplifying sample preparation. Such studies have the potential to provide insight into spatial distributions of bacterial cells on surfaces, and into the physical and chemical mechanisms that lead to nonuniformity.

Bacterial Growth, Aggregation, and Survival on AGAR Biomimetically Patterned Surfaces. Because of high moisture content ($\sim 98\%$ by weight), AGAR-BPS are inferior to natural plant tissue in terms of mechanical strength and vacuum stability. However, AGAR-BPS have two major advantages compared to PDMS and natural leaf surfaces. First, when prepared with suitably controlled nutrient mixtures, they can be used to study the effect of natural surface topography on bacterial growth and survival, and to identify interactions between nutrients and topography, using both wild-type and mutant bacteria. Second, when coupled to downstream detection capability, the enzymatic biodegradability of AGAR-BPS can provide unique capabilities to study cellular attachment, detachment, and surface effects on growth.

Traditionally, investigation of biofilm formation and development of control measures are both based on planktonic culture and volume statistics, which do not account for any topographical information, including effects of bacterial localization. However, the current consensus on bacterial biofilms is that surface topography strongly affects bacterial spatial distribution and physiological activities.^{8,16,22–25} Modern cellular and molecular technologies (e.g., flow cytometry, PCR, etc.) can provide cellular and molecular level insight into the temporal behavior and ultimately the fate, of individual bacterial cells. To explore these possibilities, we conducted several experiments to identify potential opportunities in biointerface-related research offered by coupling these approaches to biodegradable BPS.

Creating a BPS that supports bacterial growth could facilitate our understanding of how bacteria attach, proliferate, and migrate on complex plant surfaces. We used AGAR-BPS as the substratum to investigate how natural topography and nutrient level affect growth and survival of bacterial cells. Growth of *E. coli* on an unpatterned AGAR surface was compared with that on AGAR-BPS, both with 10% tryptic soy broth (TSB) supplements (Figure 5a). Traditional plate counting, which integrates over the surface, showed no significant difference between patterned and unpatterned surfaces. However, plate counting does not provide spatial distribution information on patterned surfaces. Panels a and b in Figure 6 show the distribution of bacteria on unpatterned AGAR and AGAR-BPS, respectively, after 6 h of incubation. As in the SEM experiments, the inherent heterogeneity of surface topography on the AGAR-BPS leads to a nonuniform distribution of bacterial cells, with localized zones of aggregation in the valleys.^{8,26} These results show that AGAR-BPS are compatible with bacterial growth (Figure 5), which can be monitored by traditional culture methods used to evaluate bacterial viability. More importantly, this approach provides the opportunity to study how topographical structure affects bacterial growth and spatial distribution of bacterial cells.

Several recent studies^{8,9} suggest that microstructures on plant tissue surfaces provide an environment for bacteria to grow and persist, sheltered from biotic and abiotic stressors. Protection of bacteria by and within the topographic features of plant surface microstructures can significantly reduce the efficacy of various control measures. To date, however, little visualization or understanding of such effects has been possible. Here, we use AGAR-BPS to support formation of bacterial aggregates, and

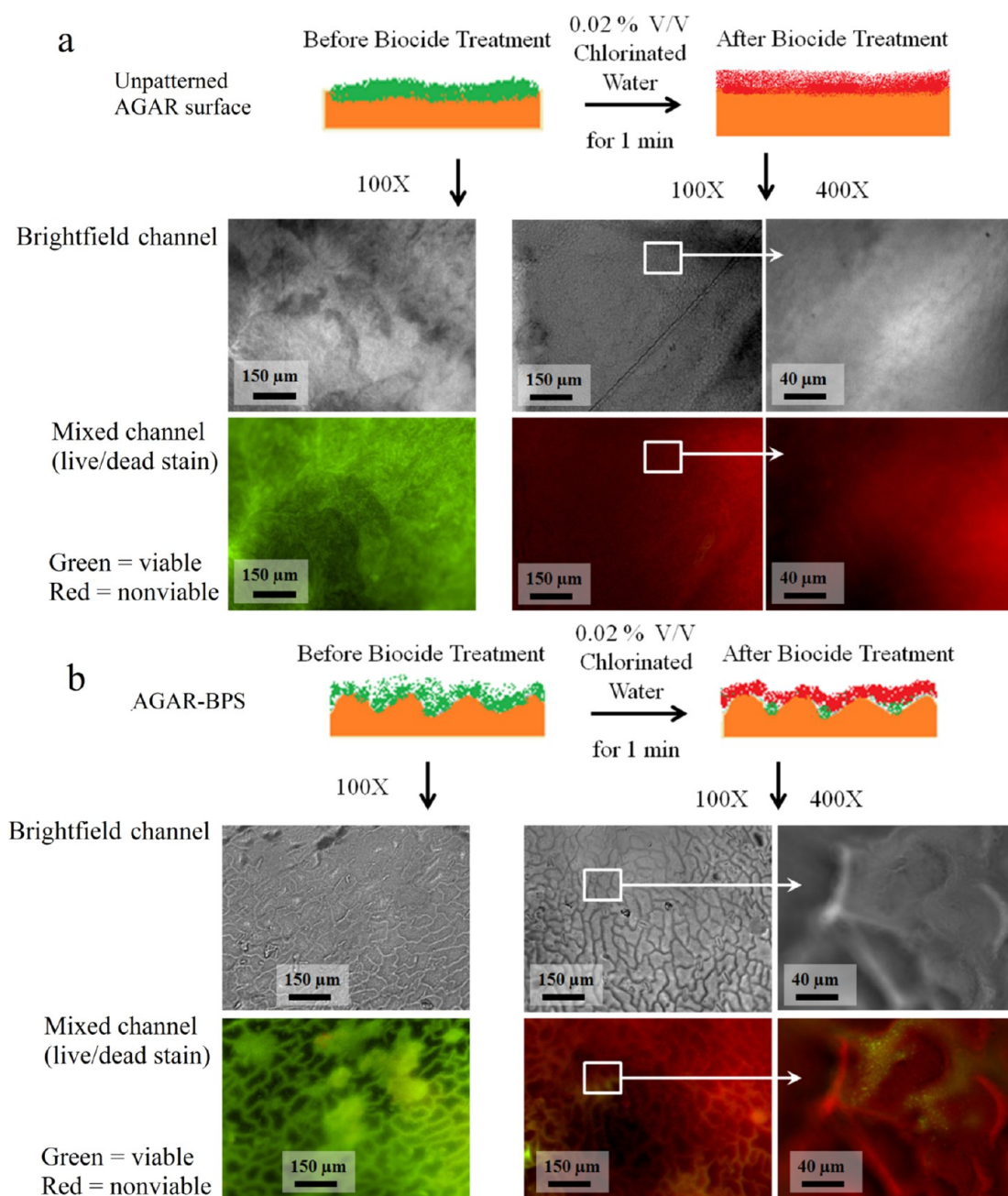


Figure 7. Effect of topography on *E. coli* survival and inactivation during a biocide treatment with 200 mg/L free chlorine for 1 min: (a) unpatterned AGAR surface; (b) AGAR-BPS. The surfaces were subjected to Live/Dead bacterial stain before and after biocide treatment. Green and red indicate live and dead bacteria, respectively.

307 then determine the effects of surface topography on bacterial
308 survival in response to dehydration and biocide treatments.

309 Nutrient supplementation of AGAR supports bacterial
310 growth, which allows investigation of bacterial survival on
311 patterned surfaces. Figure 5b shows that no later than the
312 fourth day, bacterial survival on AGAR-BPS significantly
313 exceeds survival on an unpatterned AGAR surface. These
314 results indicate that the niches on AGAR-BPS (e.g., replicated
315 valleys and stomatal structures) can offer significant protection
316 to bacterial cells against dehydration. A similar result was
317 previously reported for real plant tissue.⁸

318 Similarly, BPS can also be used to study how the topography
319 of plant surfaces influences the efficacy of biocide treatment.
320 On an unpatterned AGAR surface (Figure 7a), a relatively thick

321 bacterial growth covered the surface uniformly before biocide
322 treatment. Treatment with chlorinated water (200 mg/L for 1
323 min) killed most of the bacterial cells, and no viable cells were
324 observed in the enlarged images in Figure 7a. However, on
325 AGAR-BPS (Figure 7b) before biocide treatment, individual
326 bacterial cells are strongly clustered in the valleys, with larger
327 aggregates along the ridges. After biocide treatment with
328 chlorinated water, most bacterial cells were killed. The cell
329 aggregates were no longer observed and the background was
330 covered with red fluorescence, likely due to lysis of bacterial
331 cells during chlorine treatment. Viable cells were still observed
332 in the valleys; a result that can be attributed to the “steric”
333 protection afforded to bacterial aggregates against biocide
334 treatment.⁸ The enlarged images in Figure 7b also show a few

335 surviving bacterial cells. Besides providing information on
 336 surface topography and bacterial cell viability, AGAR-BPS can
 337 also be used for flow cytometry after enzymatic degradation, as
 338 shown schematically in Figure 1c. Results shown in Table 1

Table 1. Effects of Surface Topography on Bacterial Survival Determined by Flow Cytometry

	cell counts (log cell/cm ²) ^a			
	unpatterned AGAR surface		AGAR-BPS	
	before biocide treatment	after biocide treatment	before biocide treatment	after biocide treatment
viable counts	7.92 ± 1.01	4.42 ± 0.91	8.52 ± 1.25	6.11 ± 0.75
dead counts	5.36 ± 1.12	7.60 ± 0.88	6.40 ± 0.63	8.31 ± 1.21
reduction of viable counts	3.80 ± 0.85		2.12 ± 0.67	

^aLog cell counts are shown as mean ± standard error.

339 indicate that biocide treatment has significantly different
 340 outcomes for bacterial inactivation on unpatterned surfaces
 341 and AGAR-BPS, as expected. The biocide provides approx-
 342 imately 3.80 vs 2.12 log₁₀ reduction in viable counts on the
 343 unpatterned and patterned surfaces, respectively. Similar
 344 differential inactivation of pathogens has also been reported
 345 with real plant tissues having different surface topographies.⁸
 346 Therefore, bactericidal efficacy on BPS is lower than on
 347 chemically identical unpatterned surfaces, suggesting that
 348 topography provides “steric” protection to bacterial cells. The
 349 results also suggest the potential to combine topographical and
 350 spatial distribution information using BPS (e.g., SEM and
 351 fluorescence microscopy) and downstream flow cytometry
 352 detection.

353 The 3D distribution of bacterial cells (viable and nonviable)
 354 was also investigated by orthographic projection from Z-stack
 355 measurements using confocal microscopy. Figure 8a shows the
 356 orthographic projections of viable bacterial aggregates on
 357 AGAR-BPS before biocide treatment. In the X-Y projection,
 358 aggregates of viable bacterial cells were observed, consistent
 359 with Figure 7a. The X-Z and Y-Z projections show nearly
 360 uniform distributions of bacterial cells in the Z direction. After
 361 biocide treatment, most of the cells were dead (Figure 8b), and
 362 bacterial aggregates were no longer observed in the X-Y
 363 projection. Isolated viable cells were observed in the Z-axis in
 364 X-Z and Y-Z projections, with some in areas corresponding to
 365 valleys. This distribution strongly suggests that AGAR-BPS can
 366 provide information on how topographical features influence
 367 survival of bacterial cells.

368 ■ MATERIALS AND METHODS

369 **Materials and Chemicals.** All chemicals and buffers were
 370 purchased from Sigma-Aldrich (St. Louis, MO, USA), except for:
 371 SU-8 2050 photoresist and developer (MicroChem, Newton, MA,
 372 USA); Sylgard 184 elastomer kit (PDMS) (Dow Chemical Company,
 373 Midland, MI, USA); and agarose gel-digesting enzyme GELase
 374 (Epicenter Biotechnologies, Madison, WI, USA). Bacterial viability
 375 was determined using a Live/Dead BacLight kit (Invitrogen, Grand
 376 Island, NY, USA). Fresh spinach leaves (*Spinacia oleracea*) were
 377 purchased from a local produce wholesale market (Jessup, Md., USA).
 378 The *E. coli* cell-harboring plasmid bearing pRSET/BFP (BFP-*E. coli*)
 379 was provided by the Fischell Department of Bioengineering, University
 380 of Maryland (College Park, MD, USA).

Replica Molding of PDMS Stamps. For either PDMS or AGAR, 381
 BPS were prepared in two steps. The first step was to produce a 382
 PDMS stamp with reversed microstructure via replica molding. The 383
 second step involved thermal molding of PDMS- and AGAR-BPS 384
 from the PDMS molds (Figure 1). To prepare the PDMS molds, 385
 spinach leaves were securely taped to the bottom of a 100 mm (ID) 386
 aluminum dish. The PDMS mixture (50 g; base:curing agents =10:1) 387
 was cast in the dish, followed by degassing in low vacuum for 15 min 388
 and curing at 40 °C for 12 h. (The low curing temperature avoids 389
 thermal damage to plant tissue.) Cured PDMS stamps were then 390
 chemically modified with a layer of Pd nanoparticles (serving as a 391
 nonadhesive layer in the thermal molding step) as described below 392
 (see Figure 1a).^{18,20,27} The PDMS stamps were first oxidized for 10 393
 min in an aqueous solution containing 5.2% (v/v) hydrochloric acid 394
 (HCl) and 4.3% (v/v) hydrogen peroxide (H₂O₂) while subjected to 395
 ultrasonic treatment (35 kHz), followed by rinsing with H₂O and 396
 100% ethanol. The PDMS stamps were then treated with ultrasound 397
 for 45 min in an ethanolic solution (50%, v/v) of (3-aminopropyl) 398
 triethoxysilane (APTES) at 22 °C, followed by rinsing in ethanol and 399
 H₂O.^{18,27} The silylamine-modified PDMS was then shaken overnight 400
 at 120 rpm in 0.2 g/L of PdCl₂ in 0.2 N HCl aqueous solution, 401
 followed by 1 h treatment with 2 g/L NaH₂PO₂ aqueous solution to 402
 form the nonadhesive layer of Pd⁰ nanoparticles (Figure 1a). The Pd- 403
 coated PDMS molds were reusable, and were stored at 4 °C after each 404
 thermal molding process. 405

406 Thermal Molding of PDMS and AGAR Biomimetically

Patterned Surfaces. The PDMS- and AGAR-BPS were prepared 407
 from PDMS molds via thermal molding. The PDMS-BPS were 408
 molded and cured at 125 °C for 20 min following the manufacturer's 409
 protocol (Figure 1b). Replication of AGAR-BPS was achieved by first 410
 dissolving 2.5% (w/v) agarose (Type I–B) in water, or in 10% TSB 411
 containing 15 g/L tryptone, 5g/L soytone, and 5 g/L NaCl (Figure 412
 1c). Immediately after sterilization, 15 mL of hot liquid medium was 413
 cast on PDMS molds (preheated at room temperature and sterilized 414
 by 100% ethanol), followed by immediate low-vacuum degassing for 415
 10 s, and transfer to (and rapid gelling in) an ice bath for 5 min. After 416
 solidification, the AGAR-BPS was collected and the PDMS mold was 417
 recovered. 418

Bacterial Culture. The BFP-*E. coli* bearing pRSET/BFP plasmid 419
 was inoculated into TSB from a frozen stock culture, and incubated for 420
 24 h at 37 °C.^{28,29} Cells were harvested by centrifugation at 6000 g for 421
 10 min at 4 °C, followed by two pellet rinses with sterile phosphate 422
 buffered saline (PBS). After resuspension and dilution in PBS, each 423
 aliquot was determined to contain approximately 1 × 10⁷ CFU/mL of 424
 bacterial cells.^{8,30} 425

The bacterial attachment assays on PDMS- and AGAR-BPS were 426
 accomplished by inoculating 100 μL of the suspension containing 427
 BFP-*E. coli* over a 1 cm² area. For PDMS- BPS assays, inocula were 428
 incubated for 12 h at 37 °C, and the surface was gently rinsed with 429
 PBS for 30 s to remove loosely attached bacterial cells before further 430
 characterization. For bacterial growth studies, inoculated AGAR 431
 containing 10% TSB was incubated at 25 °C. Growth was examined 432
 by traditional plate counting as previously described^{8,30–32} and by 433
 fluorescence microscopy, at 2-h intervals for 24 h. To study bacterial 434
 survival, inoculated AGAR without nutrient supplements was 435
 incubated at 4 °C, and plate counts were recorded at 0, 1, 4, and 7 436
 days. Before each microscopic observation, bacteria on the AGAR 437
 surface were stained at 22 °C for 15 min in the dark with 500 μL of the 438
 Live/Dead bacterial viability stain. Buffer containing 6 μM SYTO 9 439
 stains live cells green and 30 μM propidium iodide stains dead cells 440
 red. After 12 h of incubation, biocide (200 mg/L chlorinated water) 441
 was applied to the surface for 1 min. The bactericidal effect was also 442
 examined using the bacterial viability staining kit. 443

Microscopy. Analyses of surface topography, roughness, and 3D 444
 imaging of spinach leaf, PDMS molds, PDMS-BPS, and AGAR-BPS 445
 were performed using a 3D digital optical microscope (Hirox KH- 446
 7700, Hackensack, NJ, USA). Specimen preparation of PDMS molds 447
 and PDMS-BPS was as previously described in the thermal molding 448
 section. AGAR-BPS were prepared by molding the sample between 449
 the PDMS mold and a glass slide, in order to limit the gel thickness to 450

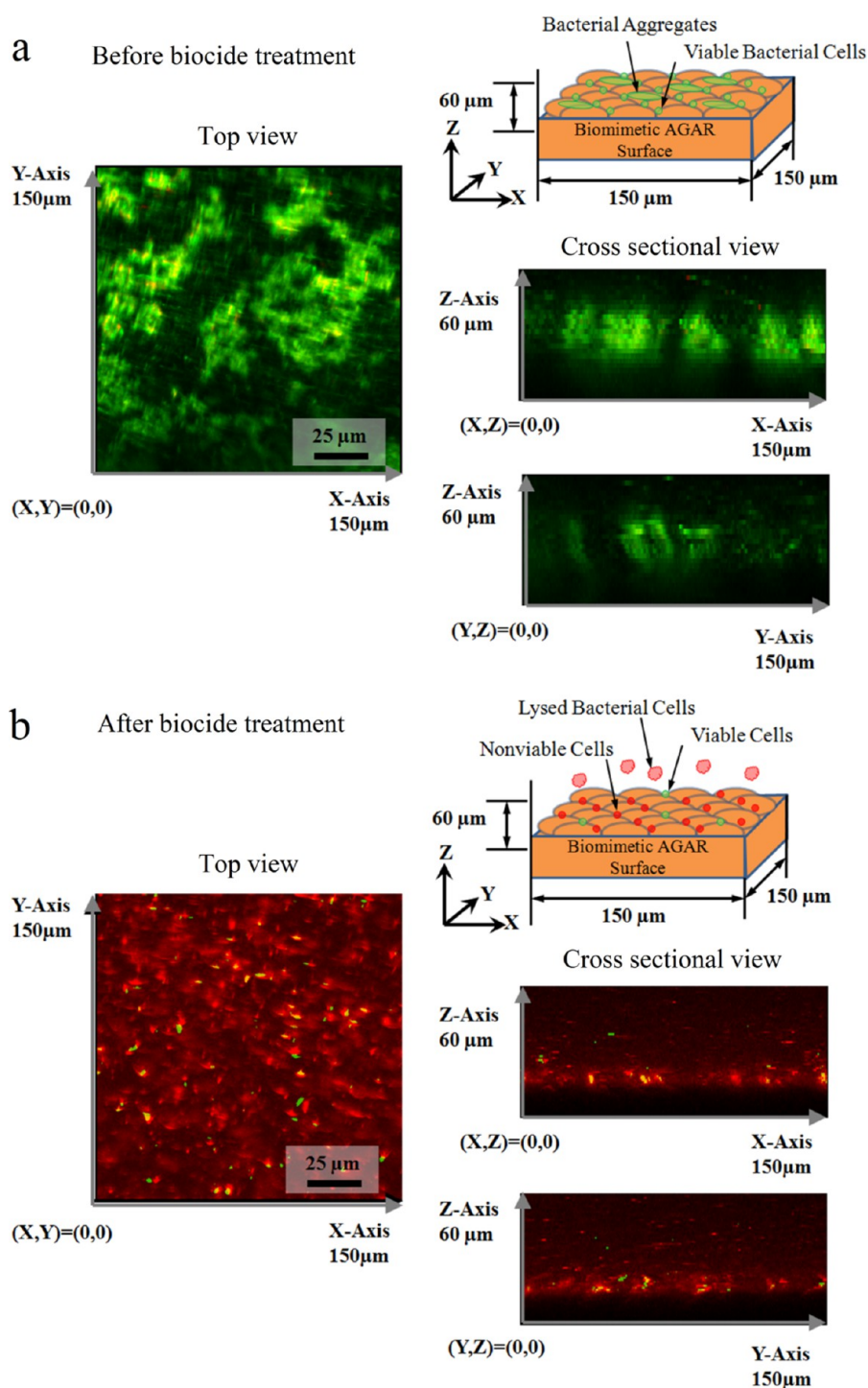


Figure 8. Images illustrating “steric” protection of bacteria in valleys on AGAR-BPS: (a) fluorescent orthographic projection ($400\times$) of *E. coli* growth and bacterial aggregates formation after 12 h of incubation; (b) fluorescent orthographic projection ($400\times$) of *E. coli* survival after biocide treatment.

451 1.5 mm and thus reduce light scattering. The magnification power was
452 $1050\times$ using an OL-350 II objective lens, with 3D rendering of surface
453 topography achieved by obtaining several image stacks ranging
454 between 0 and $50\ \mu\text{m}$ at different elevations ($1.5\ \mu\text{m}/\text{slide}$) using a
455 motorized Z-axis control. The resolution on the X- and Y-axes was
456 $0.183\ \mu\text{m}/\text{pixel}$, over an area of $300\ \mu\text{m}$ by $200\ \mu\text{m}$ (1.92 million pixels
457 in total). The data were processed with the manufacturer’s 3D
458 profilometry software (Hirox KH-7700 3D Viewer) to generate 3D
459 structural models. R_{RMS} values were calculated from the standard
460 deviation of the z-values of all pixels.

Electron microscopy images were captured utilizing a S-3700 VP- 461
SEM (Hitachi High Technologies America, Inc., Pleasanton, CA, 462
USA) with a Deben Coolstage Peltier stage (Deben UK Ltd., Suffolk, 463
UK) set at $-25\ ^\circ\text{C}$.⁹ Spinach leaves and PDMS-BPS were cut into 464
small pieces before mounting on 51 mm aluminum specimen stubs 465
using conductive carbon tape. All images were captured at $1000\times$ 466
magnification at 10 kV accelerating voltage, 10 mm working distance, 467
and 40 Pa vacuum level. 468

Fluorescent images for on-chip BFP-*E. coli* or AGAR Live/Dead cell 469
staining were observed and captured using an optical microscope 470

471 (Nikon E400, Nikon Instruments, Melville, NY, USA) with a
472 fluorescent illuminator (Intensilight C-HGFI, Nikon) and fluorescent
473 filter cubes of BFP, FITC (SYTO 9), and TRITC (for propidium
474 iodide). A Cool Snap HQ camera (Photometrics, Tucson, AZ, USA)
475 and NIS Elements software (version 3.0, Nikon) were used to visualize
476 fluorescent signals. Nikon Plan 10 \times /0.25 and Nikon Plan 40 \times /0.65
477 objective lenses, and a 10 \times ocular lens were used in the study.⁶

478 Confocal scanning microscopy (Zeiss LSM-700, Jena, Germany)
479 was used to study the role of surface topography on bacterial growth
480 and survival.⁹ The Z-stack function was used to scan a 150 μm \times 150
481 μm area at Z-axis resolution of 2 μm /slice. The excitation laser had a
482 wavelength of 488 nm, and a FITC filter was used to capture the
483 SYTO 9 signal (green fluorescence), while a PI filter was used for
484 propidium iodide stained cells (red fluorescence). An EC Plan-
485 Neofluar 40 \times /0.9 was used as the objective lens. Z-stack images were
486 analyzed and constructed using Zen software (2012, Zeiss).

487 **Contact Angle Measurement.** Contact angle measurements
488 were made by the sessile drop method using an Attension Theta
489 optical tensiometer system (Biolin Scientific, Linthicum Heights, MD,
490 USA), with a drop volume of 50 μL (5 drops on a 1 cm \times 10 cm
491 strip). Placement of drops of either water, or an aqueous solution of
492 Triton X-100 or Na-CMC, on each surface was controlled by an
493 automatic liquid dispenser (C201, Biolin Scientific). Data recording
494 (60 fps) was triggered by the initial contact of a liquid drop with a
495 solid surface (i.e., an unpatterned PDMS surface, PDMS-BPS, or
496 spinach leaf). We selected leaf portions with relatively low gross
497 curvature, which were quite flat on the scale of the relatively large
498 drops (equivalent spherical diameter of \sim 4.6 mm, and equivalent
499 hemispherical diameter of \sim 5.8 mm). For each surface type, 20
500 specimens were used. All measurements were performed with sessile
501 “advanced” drops (i.e., static drops for which the contact surface had
502 most recently advanced), under ambient conditions. Captured images
503 were analyzed automatically (OneAttension software, Version 1.8,
504 Biolin Scientific, Linthicum Heights, MD, USA) to identify the
505 baseline and calculate contact angles.

506 **Flow Cytometry.** Flow downstream of the AGAR-BPS (Figure 1c)
507 was quantified with a flow cytometer to demonstrate the possibility of
508 counting cells and monitoring their viability.³³ After microscopic
509 examination, AGAR-BPS (1 cm²) were enzymatically degraded in 10
510 mL of GELase solution (20 units/mL) at 45 $^{\circ}\text{C}$ for 40 min. Aliquots
511 of 1 mL of the resulting suspension containing live and dead bacterial
512 cells were then analyzed by flow cytometry (FACS Canto II, BD
513 Biosciences, San Jose, CA, USA) for fluorescence expression and
514 viability counts. The negative control was prepared using a bacterial
515 suspension of cells grown on an unpatterned AGAR surface, and
516 sterilizing the suspension with 200 mg/L chlorinated water for 1 min.
517 Flow cytometry data were analyzed by FACS Canto clinical software
518 (BD Biosciences, Sparks, MD) to calculate means and standard errors
519 of cell counts and survival rates.

520 **Statistical Analysis.** Surface roughness, contact angle, and flow
521 cytometry experiments were conducted with five replications, and the
522 data were reported as mean \pm standard error. Analysis of variance
523 (ANOVA) was performed using SAS software (Version 9.2, SAS
524 Institute Inc., Cary, NC). Surface roughness of PDMS molds and BPS
525 were tested against that of spinach leaf by ANOVA Dunnett's test. The
526 contact angles of water, and of the aqueous solutions of Triton X-100
527 and Na-CMC, on unpatterned PDMS, PDMS-BPS, and spinach leaves
528 were ranked using ANOVA Tukey's test. The probability (*P*) of all test
529 statistics was set at 0.05.

530 ■ COMMENTS AND CONCLUSIONS

531 In this study, a two-step replica molding method was developed
532 for rapid fabrication of polymer-based biomimetically patterned
533 surfaces (BPS) having the surface microstructure of plant tissue.
534 Surfaces of PDMS- and AGAR-BPS replicating spinach leaf
535 microstructure demonstrate a high degree of topographical
536 fidelity to the original plant tissue. PDMS surfaces provide
537 structural stability under vacuum for SEM-associated applica-
538 tions, and have surface wettability similar to natural leaf

surfaces, which will facilitate development of coating and 539
biocide-related intervention technologies. The possibility of 540
chemically functionalizing PDMS²⁷ allows for potential 541
tailoring of chemical properties important to bacterial attach- 542
ment, with independent control of microstructural topography. 543
For AGAR surfaces, simple adjustment of nutrient levels 544
facilitates investigation of how natural topography affects 545
bacterial growth and survival. Exploratory experiments show 546
that high-fidelity topography, structural stability, and the 547
capability to integrate with instrumentation for studying 548
bacterial growth and survival on PDMS- and AGAR-BPS, 549
provide potentially valuable tools for plant–bacteria interaction 550
studies, including those relevant to food safety. AGAR-BPS can 551
also be enzymatically degraded to recover bacterial cells for 552
subsequent studies using flow cytometry and other microbial 553
detection and enumeration technologies. For AGAR-based 554
BPS, the ease with which composition is modifiable provides 555
the opportunity to independently study the effects of surface 556
chemistry, microstructure, and nutrients on bacterial attach- 557
ment, growth, and survival for a wide variety of bacteria. 558

Surfaces with simple, spatially periodic microstructures in 559
which each feature has a high degree of symmetry can be 560
extremely useful for understanding certain basic mechanisms of 561
attachment. However, their use as testbeds for studying the 562
details of surface interactions (including attachment and 563
detachment) for specific bacteria/plant pairs, and in the 564
evaluation and optimization of sanitization techniques and 565
other postharvest treatments, is severely limited by the lack of 566
geometric complexity. Real plant surfaces are highly complex at 567
the micro- and nanoscale, and so the value of an approach that 568
provides for reproducible studies of geometrically complex 569
surfaces is evident. A key advantage of the present approach is 570
that it avoids two pitfalls of conventional microfabrication 571
techniques for producing geometrically complex surfaces. First, 572
existing approaches require laborious clean-room fabrication 573
processes involving multiple high-vacuum (e.g., ion sputter 574
coating) and high-temperature (e.g., nickel stamp electroplating 575
at 55–70 $^{\circ}\text{C}$) treatments.^{34–36} Second, those methods 576
reproduce plant surface structures on a self-cleaning super- 577
hydrophobic surface, which is generally incompatible with 578
cellular attachment.^{34,36,37} An additional advantage of the 579
present approach is that it allows for a relatively “clean” 580
separation of the effects of surface microstructure from those of 581
surface chemistry and nanoscale texturing, since one can 582
independently control the chemical composition and properties 583
of the polymeric surface, while maintaining identical micro- 584
structures in the replica molding process. 585

Initial applications tested in this study demonstrate the 586
robustness of biomimetically patterned surfaces and their 587
potential application to other areas of plant or animal tissue- 588
microbe interface research. Because surface biochemistry is also 589
critical to bacterial attachment, growth, and inactivation, 590
establishing biochemical similarity would be the next step. 591
Systematic evaluation of the interaction between living bacterial 592
cells and surfaces is essential to development of possible 593
interventions directed at reducing or eliminating attachment 594
and microbial survival. Although spinach leaves were chosen as 595
the plant surface in this study, the method developed has great 596
potential for replicating the surfaces of other plant and animal 597
tissues. We anticipate that this approach will provide an 598
important research tool for understanding surface–bacteria 599
interactions and facilitating development of technology to 600

601 enhance inactivation of foodborne human pathogens and
602 improve public health.

603 ■ AUTHOR INFORMATION

604 Corresponding Author

605 *E-mail: yaguang.luo@ars.usda.gov. Tel: 301.504.6186. Fax:
606 301.504.5107.

607 Notes

608 The authors declare no competing financial interest.

609 ■ ACKNOWLEDGMENTS

610 This work was supported by USDA-NIFA Specialty Crop
611 Research Initiative Grant Award 2010-01165. We also acknowl-
612 edge grant HDTRA1-13-0037 and BO08SPO008 from the U.S.
613 Defense Threat Reduction Agency. We are grateful for the
614 support of the FabLab at the Maryland NanoCenter. We thank
615 Dr. William Bentley and Ms. Jessica Terrell of the Fischell
616 Department of Bioengineering at the University of Maryland,
617 College Park, for providing BFP-*E. coli* strains and for generous
618 technical support. Access to the FACS equipment at the Flow
619 Cytometry Core Facility (Maryland Pathogen Research
620 Institute, University of Maryland) is gratefully acknowledged.

621 ■ REFERENCES

- 622 (1) CDC, CDC Estimates of Foodborne Illness in the United States
623 2011, CS218786-A.
624 (2) Lynch, M. F.; Tauxe, R. V.; Hedberg, C. W. The Growing Burden
625 of Foodborne Outbreaks due to Contaminated Fresh Produce: Risks
626 and Opportunities. *Epidemiol. Infect.* **2009**, *137*, 307–315.
627 (3) Erickson, M. C. Internalization of Fresh Produce by Food borne
628 Pathogens. *Annu. Rev. Food Sci. Technol.* **2012**, *3*, 283–310.
629 (4) Erickson, M. C.; Webb, C. C.; Diaz-Perez, J. C.; Davey, L. E.;
630 Payton, A. S.; Flitcroft, I. D.; Phatak, S. C.; Doyle, M. P. Internalization
631 of *Escherichia coli* O157:H7 Following Spraying of Cut Shoots when
632 Leafy Greens are Regrown for a Second Crop. *J. Food Prot.* **2013**, *76*,
633 2052–2056.
634 (5) Erickson, M. C.; Webb, C. C.; Diaz-Perez, J. C.; Davey, L. E.;
635 Payton, A. S.; Flitcroft, I. D.; Phatak, S. C.; Doyle, M. P. Absence of
636 Internalization of *Escherichia coli* O157:H7 into Germinating Tissue of
637 Field-Grown Leafy Greens. *J. Food Prot.* **2014**, *77*, 189–196.
638 (6) Sharma, M.; Ingram, D. T.; Patel, J. R.; Millner, P. D.; Wang, X.;
639 Hull, A. E.; Donnenberg, M. S. A Novel Approach to Investigate the
640 Uptake and Internalization of *Escherichia coli* O157:H7 in Spinach
641 Cultivated in Soil and Hydroponic Medium. *J. Food Prot.* **2009**, *72*,
642 1513–1520.
643 (7) Whitehead, K. A.; Verran, J. The Effect of Surface Topography on
644 the Retention of Microorganisms. *Food Bioprod. Process.* **2006**, *84*,
645 253–259.
646 (8) Wang, H.; Feng, H.; Liang, W.; Luo, Y.; Malyarchuk, V. Effect of
647 Surface Roughness on Retention and Removal of *Escherichia coli*
648 O157:H7 on Surfaces of Selected Fruits. *J. Food Sci.* **2009**, *74*, E8–
649 E15.
650 (9) Macarasin, D.; Patel, J.; Bauman, G.; Giron, J. A.; Ravishankar, S.
651 Effect of Spinach Cultivar and Bacterial Adherence Factors on Survival
652 of *Escherichia coli* O157:H7 on Spinach Leaves. *J. Food Prot.* **2013**, *76*,
653 1829–1837.
654 (10) Seo, K. H.; Frank, J. F. Attachment of *Escherichia coli* O157:H7
655 to Lettuce Leaf Surface and Bacterial Viability in Response to Chlorine
656 Treatment as Demonstrated by Using Confocal Scanning Laser
657 Microscopy. *J. Food Prot.* **1999**, *62*, 3–9.
658 (11) Warning, A.; Datta, A. K. Interdisciplinary Engineering
659 Approaches to Study How Pathogenic Bacteria Interact with Fresh
660 Produce. *J. Food Eng.* **2013**, *114*, 426–448.
661 (12) Apoga, D.; Barnard, J.; Craighead, H. G.; Hoch, H. C.
662 Quantification of Substratum Contact Required for Initiation of

- Colletotrichum graminicola* Appressoria. *Fungal Genet. Biol.* **2004**, *41*, 663
1–12. 664
(13) Held, M.; Edwards, C.; Nicolau, D. V. Probing the Growth
665 Dynamics of *Neurospora crassa* with Microfluidic Structures. *Fungal* 666
Biol. **2011**, *115*, 493–505. 667
(14) De la Fuente, L.; Montanes, E.; Meng, Y. Z.; Li, Y. X.; Burr, T. 668
J.; Hoch, H. C.; Wu, M. M. Assessing Adhesion Forces of Type I and 669
Type IV Pili of *Xylella fastidiosa* Bacteria by Use of a Microfluidic Flow 670
Chamber. *Appl. Environ. Microbiol.* **2007**, *73*, 2690–2696. 671
(15) Sirinutsomboon, B.; Delwiche, M. J.; Young, G. M. Attachment 672
of *Escherichia coli* on Plant Surface Structures Built by Micro- 673
fabrication. *Biosyst. Eng.* **2011**, *108*, 244–252. 674
(16) Friedlander, R. S.; Vlamakis, H.; Kim, P.; Khan, M.; Kolter, R.; 675
Aizenberg, J. Bacterial Flagella Explore Microscale Hummocks and 676
Hollows to Increase Adhesion. *Proc. Natl. Acad. Sci. U.S.A.* **2013**, *110*, 677
5624–5629. 678
(17) Seo, J.; Lee, L. P. Effects on Wettability by Surfactant 679
Accumulation/Depletion in Bulk Polydimethylsiloxane (PDMS). 680
Sens. Actuators, B **2006**, *119*, 192–198. 681
(18) Zhang, B.; Feldman, A.; Wang, Q. A Novel Insight in Rapid 682
Allergen Detection in Food Systems: from Threshold Dose to Real- 683
World Concentration. *Sens. Actuators, B* **2013**, *186*, 597–602. 684
(19) Anselme, K.; Davidson, P.; Popa, A. M.; Giazzon, M.; Liley, M.; 685
Ploux, L. The Interaction of Cells and Bacteria with Surfaces 686
Structured at the Nanometre Scale. *Acta Biomater.* **2010**, *6*, 3824– 687
3846. 688
(20) McDonald, J. C.; Duffy, D. C.; Anderson, J. R.; Chiu, D. T.; Wu, 689
H. K.; Schueller, O. J. A.; Whitesides, G. M. Fabrication of Microfluidic 690
Systems in Poly(dimethylsiloxane). *Electrophoresis* **2000**, *21*, 27–40. 691
(21) Feng, L.; Zhang, Y. A.; Xi, J. M.; Zhu, Y.; Wang, N.; Xia, F.; 692
Jiang, L. Petal Effect: a Superhydrophobic State with High Adhesive 693
Force. *Langmuir* **2008**, *24*, 4114–4119. 694
(22) Hall-Stoodley, L.; Costerton, J. W.; Stoodley, P. Bacterial 695
Biofilms: from the Natural Environment to Infectious Diseases. *Nat.* 696
Rev. Microbiol. **2004**, *2*, 95–108. 697
(23) Debeer, D.; Stoodley, P.; Roe, F.; Lewandowski, Z. Effects of 698
Biofilm Structures on Oxygen Distribution and Mass-Transport. 699
Biotechnol. Bioeng. **1994**, *43*, 1131–1138. 700
(24) Huang, C. T.; Xu, K. D.; McPeters, G. A.; Stewart, P. S. Spatial 701
Patterns of Alkaline Phosphatase Expression within Bacterial Colonies 702
and Biofilms in Response to Phosphate Starvation. *Appl. Environ.* 703
Microbiol. **1998**, *64*, 1526–1531. 704
(25) Rizzello, L.; Sorce, B.; Sabella, S.; Vecchio, G.; Galeone, A.; 705
Brunetti, V.; Cingolani, R.; Pompa, P. P. Impact of Nanoscale 706
Topography on Genomics and Proteomics of Adherent Bacteria. *ACS* 707
Nano **2011**, *5*, 1865–1876. 708
(26) Lawrence, J. R.; Korber, D. R.; Hoyle, B. D.; Costerton, J. W.; 709
Caldwell, D. E. Optical Sectioning of Microbial Biofilms. *J. Bacteriol.* 710
1991, *173*, 6558–6567. 711
(27) Yu, L.; Li, C.; Liu, Y. S.; Gao, J.; Wang, W.; Gan, Y. Flow- 712
through Functionalized PDMS Microfluidic Channels with Dextran 713
Derivative for ELISAs. *Lab Chip* **2009**, *9*, 1243–1247. 714
(28) Tsao, C. Y.; Hooshangi, S.; Wu, H. C.; Valdes, J. J.; Bentley, W. 715
E. Autonomous Induction of Recombinant Proteins by Minimally 716
Rewiring Native Quorum Sensing Regulon of *E. coli*. *Metab. Eng.* **2010**, 717
12, 291–297. 718
(29) Cheng, Y.; Luo, X. L.; Tsao, C. Y.; Wu, H. C.; Betz, J.; Payne, G. 719
F.; Bentley, W. E.; Rubloff, G. W. Biocompatible Multi-Address 3D 720
Cell Assembly in Microfluidic Devices using Spatially Programmable 721
Gel Formation. *Lab Chip* **2011**, *11*, 2316–2318. 722
(30) Shen, C.; Luo, Y.; Nou, X.; Bauman, G.; Zhou, B.; Wang, Q.; 723
Millner, P. Enhanced Inactivation of *Salmonella* and *Pseudomonas* 724
Biofilms on Stainless Steel by Use of T-128, a Fresh-Produce Washing 725
Aid, in Chlorinated Wash Solutions. *Appl. Environ. Microb.* **2012**, *78*, 726
6789–6798. 727
(31) Zhang, B.; Luo, Y.; Wang, Q. Development of Silver-Zein 728
Composites as a Promising Antimicrobial Agent. *Biomacromolecules* 729
2010, *11*, 2366–2375. 730

- 731 (32) Zhang, B.; Luo, Y.; Wang, Q. Development of Silver/Alpha-
732 Lactalbumin Nanocomposites: A New Approach to Reduce Silver
733 Toxicity. *Int. J. Antimicrob. Agents* **2011**, *38*, 502–509.
- 734 (33) Gupta, A.; Terrell, J. L.; Fernandes, R.; Dowling, M. B.; Payne,
735 G. F.; Raghavan, S. R.; Bentley, W. E. Encapsulated Fusion Protein
736 Confers "Sense and Respond" Activity to Chitosan-Alginate Capsules
737 to Manipulate Bacterial Quorum Sensing. *Biotechnol. Bioeng.* **2013**,
738 *110*, 552–562.
- 739 (34) Lee, S. M.; Kwon, T. H. Mass-producible Replication of Highly
740 Hydrophobic Surfaces from Plant Leaves. *Nanotechnology* **2006**, *17*,
741 3189–3196.
- 742 (35) Lee, S. M.; Upping, J.; Bielawny, A.; Knez, M. Structure-Based
743 Color of Natural Petals Discriminated by Polymer Replication. *ACS*
744 *Appl. Mater. Interfaces* **2011**, *3*, 30–34.
- 745 (36) Liu, B.; He, Y. N.; Fan, Y.; Wang, X. G. Fabricating Super-
746 hydrophobic Lotus-leaf-like Surfaces through Soft-lithographic Im-
747 printing. *Macromol. Rapid Commun.* **2006**, *27*, 1859–1864.
- 748 (37) Lampin, M.; Warocquier-Clerout, R.; Legris, C.; Degrange, M.;
749 Sigot-Luizard, M. F. Correlation between Substratum Roughness and
750 Wettability, Cell Adhesion, and Cell Migration. *J. Biomed. Mater. Res.*
751 **1997**, *36*, 99–108.